Identification of Quinone Methide Metabolites of Dauricine in Human Liver Microsomes and in Rat Bile

Yuya Wang,[†] Dafang Zhong,[†] Xiaoyan Chen,*[,†] and Jiang Zheng*[,‡]

Shanghai Institute of Materia Medica, Chinese Academy of Sciences, Shanghai, China, and Center for Developmental Therapeutics, Seattle Children's Hospital Research Institute, Division of Gastroenterology, Department of Pediatrics, University of Washington, Seattle, Washington 98195-6320

Received October 26, 2008

Dauricine is one type of the bisbenzyltetrahydroisoquinoline alkaloid derivative with antiarrhythmic effects. Severe liver toxicity was observed in experimental animals treated with analogues of dauricine, which may be caused by covalent binding of reactive metabolite(s) to critical macromolecules in tissues. The study described herein aimed at characterizing pathways of dauricine bioactivation and the CYP enzyme involved. In incubations of dauricine with NADPH- and GSH-supplemented human liver microsomes, four GSH conjugates with $[M + H]^+$ ions at *m/z* 930, 916, 916, and 902, respectively, were detected by liquid chromatography-ion trap mass spectrometry. The structures of the four metabolites were determined to be GSH conjugates of dauricine, 2-*N*-demethyl dauricine, 2′-*N*-demethyl dauricine, and *N*-demethyl-*O*-demethyl dauricine. GSH conjugation took place with a strong preference at C-17, suggesting that the phenol moiety of dauricine and its metabolites underwent oxidation to quinone methide intermediates. The formation of the GSH conjugates was found to require the presence of NADPH. To identify the CYP isoforms that are responsible for bioactivation, dauricine was also incubated with recombinant human CYP450 enzymes. The formation of GSH was only observed with the incubation of CYP3A4. In addition, the level of these GSH conjugates in human microsomes was reduced upon the addition of a CYP3A4 inhibitor ketoconazole. The same GSH conjugates were also observed in rat bile following a single oral dose of 40 mg/kg dauricine. These studies suggest that the CYP3A4 mediated quinone methide formation was associated with dauricine bioactivation.

Introduction

Bisbenzylisoquinoline alkaloids are naturally occurring phytochemicals that are common constituents of hundreds of plant species around the world. More than 400 bisbenzylisoquinoline alkaloids have been identified mainly among the following four families: Menispermaceae, Berberidaceae, Ranunculaceae, and Annonaceae (*1*). These alkaloids have received great attention due to their wide range of pharmacological activities, including anti-inflammatory, cardiovascular, membrane modulatory, P-glycoprotein modulatory, platelet aggregation inhibition, and cancer-preventive effects (*1*−*9*).

Dauricine (Table 1), a bisbenzylisoquinoline alkaloid, is the major bioactive component isolated from the root of *Dauricum D.C.*, which has been commonly used in traditional Chinese medicine as a remedy for the treatment of throat swelling, amygdalitis, and chronic bronchitis (*10*). In recent years, dauricine has attracted substantial attention due to its antiarrhythmic effects observed in several experimental arrhythmic animal models and in cardiac arrhythmic patients (*3, 11*−*13*).

Both phase I and phase II metabolism of dauricine have been observed in in vitro and in vivo animal studies (*14, 15*). *N*-Demethylated dauricine was reported as the major metabolite both in vitro and in vivo (*14*). The other phase I metabolic pathways of dauricine observed include hydroxylation and dehydrogenation. Urinary phase II metabolites of dauricine were also identified, and they were glucuronic acid and sulfate conjugates (*15*). Han and co-workers (*15*) detected dehydrogenated dauricine excreted in the urine of animals receiving

Table 1. Chemical Structures of Dauricine (I), 2-*N*-Demethyldauricine (II), Daurisoline (III), Dauricinoline (IV), Dauricicoline (V), and GSH Conjugate of Dauricine (VI)

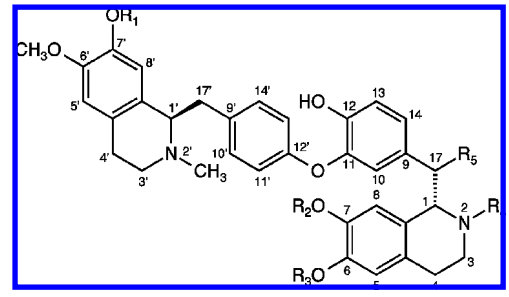

	name	R_1	R_2	R_3	R_4	R_5
I	dauricine	CH_3	CH_3	CH_3	CH_3	H
II	2-*N*-demethyldauricine	CH_3	CH_3	CH_3	H	H
III	daurisoline	CH_3	H	CH_3	CH_3	H
IV	dauricinoline	CH_3	CH_3	H	CH_3	H
V	dauricicoline	H	CH_3	H	CH_3	H
VI	GSH conjugate of dauricine	CH_3	CH_3	CH_3	CH_3	GS[a]

[a] Glutathione.

* To whom correspondence should be addressed. (X.Y.C) Tel/Fax: +86-21-50800738. E-mail: xychen@mail.shcnc.ac.cn. (J.Z.) Tel: (206) 884-7651. Fax: (206) 987-7660. E-mail: jiang.zheng@Seattlechildrens.org.

[†] Shanghai Institute of Materia Medica.

[‡] University of Washington.

10.1021/tx800397e CCC: $40.75
Published on Web 04/09/2009

dauricine by liquid chromatography/ion trap mass spectrometry (LC/MS^n),[1] but they were unable to characterize the structures of such dehydrogenated dauricine metabolites. In this study, we report the isolation and characterization of a quinone methide metabolite of dauricine. In addition, we report that the formation of the quinone methide metabolite is catalyzed by CYP3A4. Quinone methides are known as electrophilic species, and the finding of the quinone methide metabolite of dauricine sounds an alarming note for the safe of consumption of bisbenzylisoquinoline alkaloid-related natural products.

Materials and Methods

Materials. Dauricine (**I**), 2-*N*-demethyl dauricine (**II**), daurisoline (**III**), dauricinoline (**IV**), dauricicoline (**V**), and tetrandrine were purchased from Shenzhen Medherb Bio-Tech Co., Ltd. (Shenzhen, Guangdong, China) (Table 1). All purities were >98%. The following chemicals were purchased from Sigma-Aldrich (St. Louis, MO, USA): GSH, NADPH, α-naphthoflavone, pilocarpine, sulfaphenazole, ticlopidine, quinidine, and ketoconazole. Pooled human liver microsomes and recombinant CYP enzymes CYP1A2, 2A1, 2C9, 2C19, 2D6, 2E1, and 3A4 were purchased from BD Gentest (Woburn, MA, USA). The concentrations of the recombinant enzymes were all 50 nM in 100 mM potassium phosphate buffer (pH 7.4). All other reagents and solvents were of either analytical or HPLC grade.

Synthesis of Dauricine GSH Conjugate. To the solution of dauricine (60 mg, 0.066 mmol) in benzene (15 mL) at 5−10 °C, 2,3-dichloro-5,6-dicyano-1,4-benzoquinone (DDQ, 16.5 mg, 0.72 mmol) was slowly added, and the reaction mixture was stirred for 10 min (*16*), followed by the addition of glutathione (20.5 mg, 0.066 mmol), H_2O (3.0 mL), and tetrahydrofuran (3.0 mL). After stirring for 24 h at room temperature, the reaction mixture was diluted with 30 mL of H_2O. The aqueous layer was lyophilized to give a crude solid product (42 mg), which was then subjected to purification by a Waters 2545 semipreparative HPLC system (Waters Corporation, Milford, MA, USA) on a Shim-pack PRC-ODS column (250 × 20 mm i.d., Shimadzu, Kyoto, Japan) using methanol and H_2O (30:70, v/v) as the mobile phase at the flow rate of 3.0 mL/min to obtain 24 mg of the GSH conjugate. Its structure was characterized by high resolution mass spectrometry and NMR. The high resolution MS experiments were carried out on an LTQ/Orbitrap mass spectrometer (Thermo Fisher Scientific, Bremen, Germany). The parameters of positive ESI source were as follows: ionization voltage 3.5 kV, capillary temperature 275 °C, mass accuracies <3 ppm, acquisition time 0.5 s/scan, activation time 30 ms, and activation parameter (*q*) 0.25. All NMR spectra were recorded on Bruker DRX 500 NMR spectrometer (Newark, DE, USA) operated at 500 MHz. Dauricine and its GSH conjugate were dissolved in deuterated methanol. Chemical shifts are expressed as parts per million relative to tetramethylsilane.

Instrumentation. The qualitative metabolic profiling was carried out on an Agilent 1200 HPLC system coupled with a 6330 LC/MSD Trap XCT Ultra (Agilent Technologies, Waldbronn, Germany). Separation was achieved using a Zorbax SB−C_{18} column (150 × 4.6 mm i.d., 5 μm; Agilent, Wilmington, DE, USA) protected by a 4.0 × 3.0 mm i.d. Security-Guard (5 μm) C_{18} column (Phenomenex, Torrance, CA, USA). The mobile phase was a gradient of a mixture of (A) methanol and (B) 5 mM ammonium acetate programmed as follows: initial 20% A maintained for 5 min, then increased to 30% in 0.5 min, maintained at 30% for 10 min, then increased to 40% in 0.5 min, maintained at 40% for 5 min, then increased to 60% in 0.5 min, maintained at 60% for 5 min and finally decreased to 20% A in 0.5 min, and maintained at 20% A for 10 min. The flow rate was 0.6 mL/min, and the injection volume was 20 μL. The HPLC effluent going to the mass spectrometer was directed to waste through a divert valve for the initial 5 min after sample injection. The mass spectrometer was equipped with an ESI source. The ionization mode was positive. The interface and MS parameters were as follows: nebulizer pressure, 40 psi (N_2); dry gas, 12 mL/min (N_2); dry gas temperature, 350 °C; spray capillary voltage, 3500 V; skimmer voltage, 40 V; ion transfer capillary exit, 124 V; scan range, *m*/*z* 150−1300; spectra average, 3; target, 200,000. For MS^n spectra, the fragmentation amplitude varied between 0.4 and 0.9 V. Other parameters, including the potentials of octapole offset and the tube lens offset, were also optimized for maximum abundance of the ions of interest by the automatic tune procedure of the instrument. The multistage mass spectra (MS^n) were produced by collision induced dissociation (CID) of the protonated molecules $[M + H]^+$ of all analytes at their respective HPLC retention times. Data acquisition was performed in full-scan LC/MS and MS^n modes ($n = 2$ or 3). All data acquired were processed by Agilent Chemstation Rev. B. 01.03 software (Agilent, Palo Alto, CA, USA).

Quantitative analysis of dauricine and its GSH conjugate in kinetic study was completed under the same LC/MS^n conditions described above. Tetrandrine, a dauricine analogue, (MW = 622, 5.0 μg/mL in methanol), was added as an internal standard during sample preparation. Calibration curves were prepared by plotting appropriate peak-area ratios (each analyte/internal standard) against analyte concentrations using $1/x^2$ weighting. The concentration of each analyte was determined by interpolation from the standard curve. The linear range of each analyte for each assay varied from 0.010 to 10.0 μg/mL.

Enzyme Incubations. All incubations were performed at 37 °C in a water bath shaker. Stock solution of dauricine was prepared in methanol. The final concentration of methanol in the incubation was 0.2% (v/v). Pooled human liver microsomes (HLMs) and the human recombinant CYP450 enzymes, including CYPs 1A2, 2A1, 2C9, 2C19, 2D6, 2E1, and 3A4 (50 nM) were carefully thawed on ice prior to the experiment. Dauricine (10 μM) was individually mixed with HLM proteins (1 mg/mL) in 100 mM potassium phosphate buffer (pH 7.4) supplemented without or with GSH at a final concentration of 5 mM. The total incubation volume was 200 μL. After 3 min of preincubation at 37 °C, the incubation reactions were initiated by the addition of NADPH (1.0 mM). After 60 min of incubation, the reactions were terminated with equal volumes of ice-cold acetonitrile. Incubations with the recombinant CYP enzymes were performed by following a protocol similar to that described above except that liver microsomes were substituted by the human recombinant CYP enzymes. Control samples containing no NADPH or substrates were included. Each incubation was performed in duplicate. For the positive scanning of GSH conjugates, samples were prepared by the precipitation of proteins as described below, prior to LC/MS^n analysis.

Microsomal Incubations in the Presence of Inhibitors. The effect of specific inhibitors of individual CYP enzymes on the formation of reactive metabolites was examined using pooled human liver microsomes. Incubation mixtures consisted of dauricine (10 μM), individual chemical inhibitors, GSH (5 mM), and pooled human liver microsomes (1 mg/mL). The CYP450-specific inhibitors α-naphthoflavone (1 μM), pilocarpine (1 μM), sulfaphenazole (1 μM), ticlopidine (0.1 μM, 1.0 μM, and 10 μM), quinidine (2 μM), and ketoconazole (0.1 μM, 1 μM, and 10 μM) were used to investigate the involvement of CYP1A2, CYP2A1, CYP2C9, CYP2C19, CYP2D6, and CYP3A4, respectively. Incubations containing dauricine were started with the addition of 1 mM NADPH, and the reactions were terminated by equal volumes of ice-cold acetonitrile. Controls containing no chemical inhibitors were included. Each incubation was performed in duplicate. Formation of metabolites was analyzed by LC/MS^n as previously described. A comparison was made relative to the controls without inhibitor, and CYP450 activity was expressed as the percentage of control activity. The choice of inhibitor concentrations was

[1] Abbreviations: COSY, correlation spectroscopy; CYP, cytochrome P450; EIC, extracted ion chromatogram; ESI, electrospray ionization; GSH, glutathione; HLMs, human liver microsomes; HMBC, heteronuclear multiple-bond correlation; HSQC, heteronuclear multiple quantum coherence; LC/MS^n, liquid chromatography/ion trap mass spectrometry; TIC, total ion chromatogram.

determined by referring to the FDA Guidance for Industry on Drug Interaction Studies (*17*).

Kinetics Study. Dauricine (1−200 μM) was incubated in human liver microsomes (0.5 mg/mL) or recombinant CYP3A4 enzyme (50 nM) in 100 mM potassium phosphate buffer (pH 7.4) containing 5 mM GSH. The total incubation volume was 200 μL. After preincubation for 3 min at 37 °C, the reaction was initiated by the addition of 1.0 mM NADPH, and was terminated with equal volumes of ice-cold acetonitrile after 60 min of incubation. All data points represent the means of duplicate estimations. K_m and V_{max} values were determined by nonlinear least-squares regression analysis using SigmaPlot software (SPSS Inc., Chicago, IL, USA).

Animal Experiments. Experiments were performed according to procedures approved by the Animal Care and Use Committee of Shanghai Institute of Materia Medica (Shanghai, China). Four male Sprague−Dawley rats (200 ± 20 g), purchased from Shanghai SLAC Laboratory Animal Co., Ltd. (Shanghai, China), were allowed free access to commercial rat chow and water. After fasting for 12 h with free access to water prior to the experiment, the animals were anesthetized with ether, and their bile ducts were cannulated with PE-10 tubing. Control bile was collected before treatment. An aqueous CMC-Na solution (0.3%) of dauricine was administered at 40 mg/kg by oral gavage, and bile was collected in Eppendorf tubes for 24 h following dosing. During the experiment, the rats were allowed free access to food and water.

Preparation of Samples for LC/MS^n Analysis. For qualitative analysis, to a 200 μL aliquot of in vitro incubations or bile collected from experimented rats, 400 μL of methanol was added. This sample was vortex-mixed and centrifuged at 11,000*g* for 5 min. The supernatant was transferred into a glass tube, evaporated to dryness under a stream of nitrogen at 40 °C, and then reconstituted in 100 μL of methanol with 5 mM ammonium acetate (30: 70, v/v). A 20 μL aliquot of the reconstituted solution was injected into the LC/MS^n system for analysis.

For quantitative analysis, a 50 μL aliquot of the IS solution (tetrandrine, 5.0 μg/mL), 50 μL of methanol−water (50: 50, v/v), and 100 μL of methanol were added to 50 μL of in vitro incubations. The resulting sample was vortex-mixed and centrifuged at 11,000*g* for 5 min. The supernatant was transferred into a glass tube, evaporated to dryness under a stream of nitrogen at 40 °C, and then reconstituted in 100 μL of methanol with 5 mM ammonium acetate (30: 70, v/v). A 20 μL aliquot of the reconstituted solution was injected to LC/MS^n system for analysis.

Results

The foundation for metabolite identification using the LC/MS^n approach is to first have a comprehensive understanding of the fragmentation behavior of the parent compound tested. Because of the two tertiary amine moieties in the structure of dauricine, the protonated molecule $[M + H]^+$ at *m/z* 625 and doubly charged ion $[M + 2H]^{2+}$ at *m/z* 313 were both observed. The intensity of $[M + 2H]^{2+}$ was less than that of $[M + H]^+$ (Figure 1). In the MS/MS spectrum (Figure 1), dauricine displayed diagnostic fragments at *m/z* 420 and *m/z* 206 formed by the cleavage of the C1−C17 or C1′−C17′ bond and the relatively stable fragment ions formed by the elimination of CH_3NH_2 (−31 Da with a proton shift) and $CH_3N{=}CH_2$ (−43 Da with a proton shift).

With the structure of *para*-methylene phenol in dauricine and its *N*-demethyl metabolites, it is speculated that they may be metabolized to quinone methide intermediates, a known electrophilic species reactive to nucleophiles, such as glutathione (GSH). As an initial step, we searched common demethylated and hydroxylated metabolites of dauricine after exposure to NADPH-supplemented human liver microsomes, using an ion trap mass spectrometer. The characteristic fragment ions from the phase I metabolites would be helpful to characterize quinone methide metabolites of dauricine.

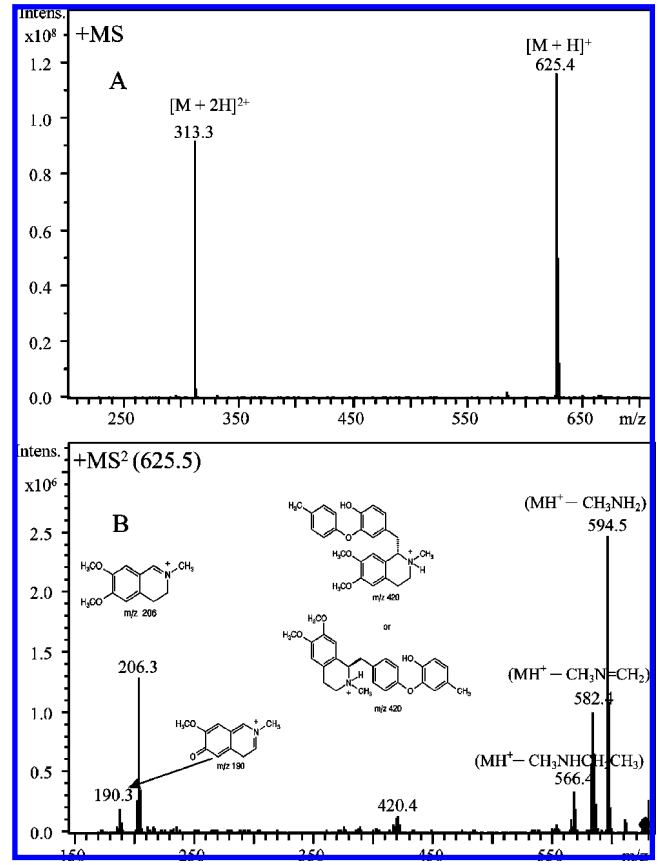

Figure 1. Full scan mass spectrum (A) and MS/MS spectrum (B) of dauricine.

Detection of Demethylated and Hydroxylated Metabolites of Dauricine in Human Liver Microsomes. Compared with the blank sample, 15 metabolites were discovered in the incubation of dauricine with human liver microsomes (Figure 2). These metabolites may be mainly classified as five types, dehydrogenated (M1-2 and M1-3, *m/z* 623), bis-dehydrogenated (M2, *m/z* 621), demethylated (M3-1, M3-2, M3-3, and M3-4, *m/z* 611), bis-demethylated (M4, *m/z* 597), and hydroxylated (M5-1, M5-2, M5-3, M5-4, M5-5, M5-6, and M5-7, *m/z* 641) metabolites. In addition, M1-1 and M1-4 were identified as the in-source fragment ions from M5-3 and M5-5 (*m/z* 641, hydroxylated metabolites) due to the loss of H_2O (18 Da), not as dehydrogenated metabolites, according to chromatographic retention times and MS/MS spectra. It was also found that M1-2 and M1-3 did not react with GSH after 60 min of incubation by comparing their peak areas in the presence or absence of GSH, indicating that these two dehydrogenated metabolites are not electrophilic.

By comparison with authentic standards, the locations of demethylation for these metabolites were proposed as follows. In the MS/MS spectra of M3-3 and M3-4, a neutral loss of 17 Da (NH_3) was observed, indicating that the *N*-demethyl moieties remained in the two metabolites (data not shown). The sites of demethylation in M3-1 to M3-4 were determined by comparing their chromatographic behavior and mass spectrometric characteristics with those of authentic 2-*N*-demethyl dauricine (II), daurisoline (III, 7-*O*-demethylated dauricine), and dauricinoline (IV, 6-*O*-demethylated dauricine). Metabolites M3-2 and M3-3 were identified to be daurisoline and 2-*N*-demethyl dauricine, respectively. Because of only two tertiary amine moieties in the structure of dauricine, M3-4 was exclusively assigned as 2′-*N*-demethyl dauricine. Metabolite M3-1 was considered as

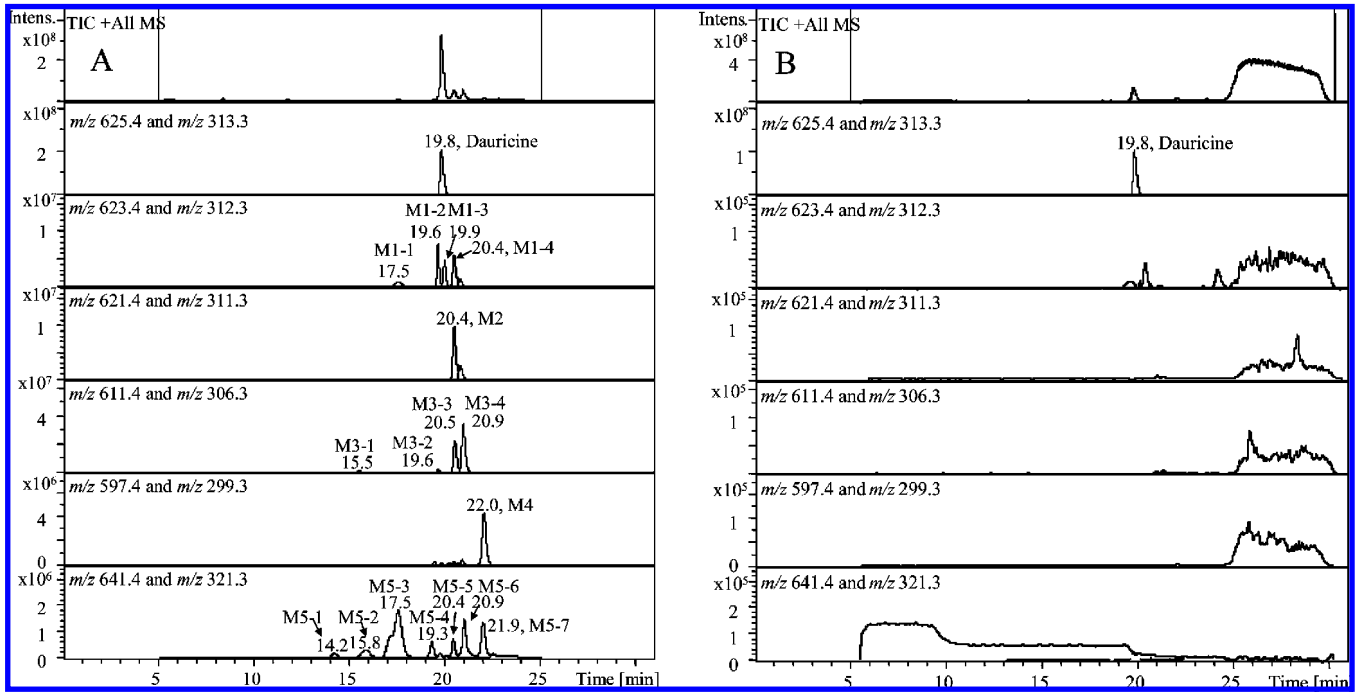

Figure 2. Extracted ion $[M + H]^+$ and $[M + 2H]^{2+}$ chromatograms of dauricine metabolites in human liver microsomal incubations. (A) With NADPH; (B) without NADPH. The detected metabolites are labeled as M1-M5, and the parent compound is labeled as dauricine.

an *O*-demethylated dauricine, but not dauricinoline. The exact structure of M3-1 needs to be further characterized.

Further mass spectrometry analyses indicated that one of the two *N*-methyl groups was retained in M4 because of the observed neutral losses of 17 Da (NH_3) and 31 Da (CH_3NH_2) in its MS/MS spectrum. Therefore, M4 was most likely an *N*-demethyl-*O*-demethyl dauricine, not bis-*O*-demethyl dauricine (dauricicoline, V). The proposed metabolic pathways of dauricine in human liver microsomes are shown in Scheme 1.

Trapping Quinone Methide Metabolites of Dauricine with GSH. The rationale for the identification of quinone methide metabolites lies in the trapping of reactive quinone methide species with a nucleophile. Nucleophilic GSH (5 mM) was incorporated as an exogenous agent to trap quinone methide metabolites of dauricine in incubations of NADPH-supplemented human liver microsomes. LC/MS^n analyses of the incubation mixture indicated that there were four GSH conjugates formed, including M6 ($[M + H]^+$, *m/z* 930, and $[M + 2H]^{2+}$, *m/z* 466, t_R = 11.7 min); M7-1 ($[M + H]^+$, *m/z* 916, and $[M + 2H]^{2+}$, *m/z* 459, t_R = 11.5 min); M7-2 ($[M + H]^+$, *m/z* 916, and $[M + 2H]^{2+}$, *m/z* 459, t_R = 13.3 min); and M8 ($[M + H]^+$, *m/z* 902, and $[M + 2H]^{2+}$, *m/z* 452, t_R = 13.1 min). Among these four conjugates, M6 was the most abundant on the basis of the peak height. The formation of M6 to M8 in these incubations was all NADPH-dependent, as illustrated by the representative chromatograms from human liver microsomal incubations (Figure 3). These data suggested that the cytochromes P450-mediated oxidative metabolism of dauricine produces varieties of quinone methide metabolites.

Characterization of GSH Conjugates of Dauricine (M6 to M8). LC/MS^n analysis of the peak responsible for M6 at the retention time of 11.7 min displayed a protonated molecule $[M + H]^+$ at *m/z* 930 and its doubly charged ion $[M + 2H]^{2+}$ at *m/z* 466 (Figure 4A), 305 Da higher than those of the parent drug, which indicated an addition of one molecule of GSH to dauricine. The MS/MS of the ion at *m/z* 930 displayed product ions of 801 (−129 Da, −pyroglutamate), 657 (−273 Da, −(GSH − H_2S)), and 623 (−307 Da, −GSH) (Figure 4B). The MS^3 spectrum of M6 (930→623) showed fragment ions of 592 (−31 Da, $-CH_3NH_2$), 580 (−43 Da, $-CH_3N{=}CH_2$), 564 (−59 Da, $-CH_3NHCH_2CH_3$), and 206 (Figure 4C) where the neutral losses were coincident with those of MS/MS of dauricine (Figure 1B). Accurate mass measurements performed with LTQ/Orbitrap mass spectrometry supported the assignment of fragment ions of dauricine and M6 (Table 2). According to the multistage MS data, the structure of M6 was proposed as the dauricine-derived GSH conjugate. The exact structure of M6 was determined by NMR and mass spectrometry below.

Dauricine was oxidized to dehydrodauricine using DDQ, followed by the addition of excess of GSH. The resulting dauricine-SG showed the same retention time (t_R), protonated molecule, and fragmentation pattern as those of M6 observed in the microsomal incubation study. The purified dauricine-SG was further characterized with 1D and 2D NMR spectroscopy, including ^{1}H NMR, ^{13}C NMR, COSY, HSQC, and HMBC, and chemical shifts and correlations were compared to a reference sample of dauricine. Table 3 lists partial ^{1}H- and ^{13}C NMR data of the dauricine-SG and authentic dauricine, and Figures S1A−C available in Supporting Information show the ^{1}H NMR, ^{13}C NMR, and ^{1}H-^{1}H COSY spectra of the parent dauricine. The protons are numbered according to the carbon to which they are attached.

Figure 5A shows the ^{1}H-^{1}H COSY spectrum of the dauricine-SG. A total of 11 aromatic protons were observed, including four singlet protons at δ_H 5.89, 6.12, 6.71, and 6.92 ppm, an AA′BB′ system at δ_H 6.67 and 7.13 ppm, and an ABX system at δ_H 6.62, 7.06, and 7.20 ppm, and no aromatic proton was missing, which excludes the possibility of GSH conjugation on the aromatic rings. As shown in Figure 5A and Table 3, the chemical shift of H-17 coupled with H-1 migrated from δ 2.65/3.15 ppm (dauricine) to 4.45 ppm (dauricine-SG), implying that an electron-withdrawing group, most likely the sulfur of GSH, was introduced to C-17. Similar chemical shift migration of C-17 from 26.5 ppm (dauricine) to 55.1 ppm (dauricine-SG) was observed in the HSQC spectra of dauricine and dauricine-SG as shown in

Scheme 1. Proposed Metabolic Pathways of Dauricine Following Incubation with Human Liver Microsomes in the Presence of NADPH

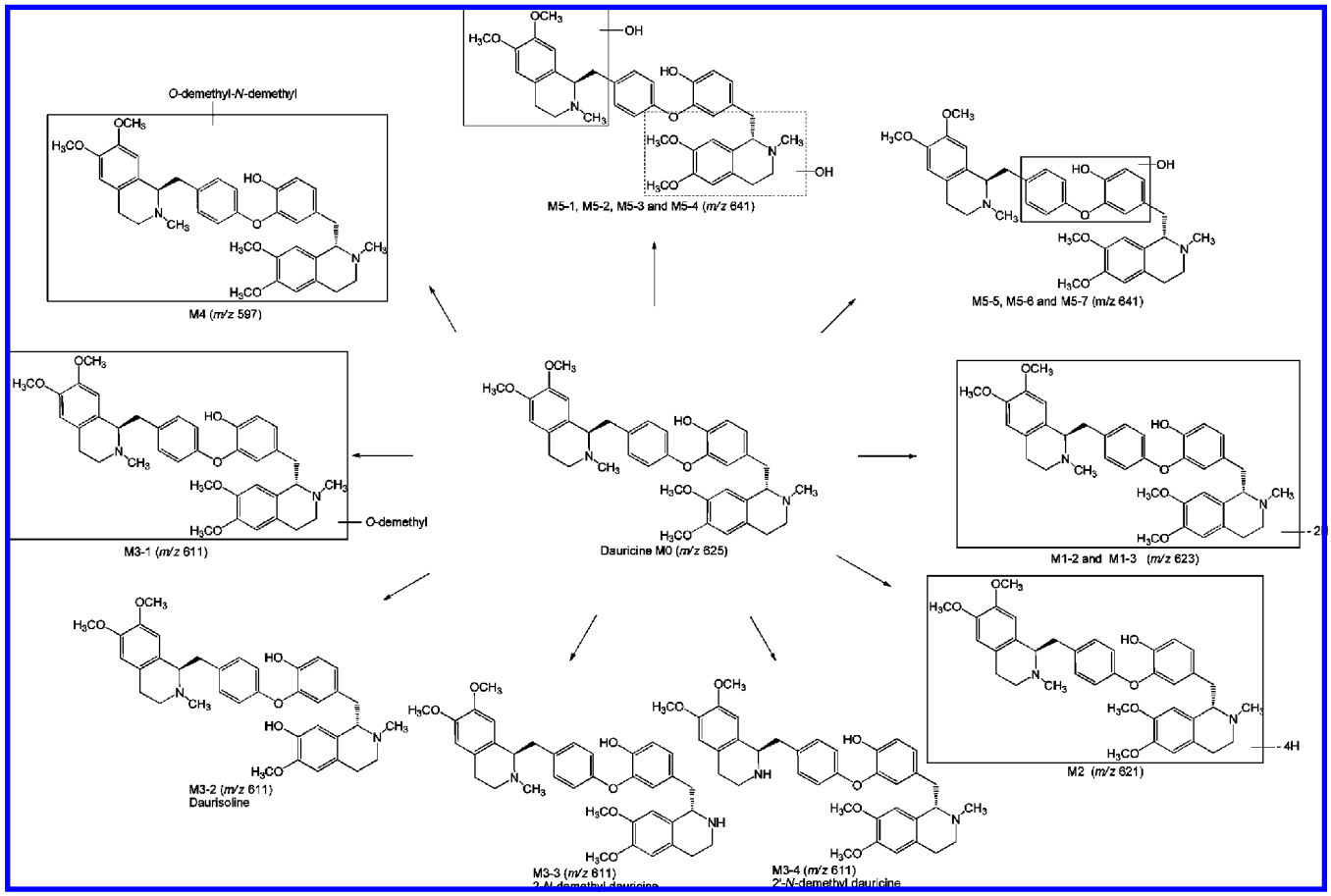

Table 3 and Figure S2 (refer to Supporting Information). The long-range coupling of C-17 (55.1 ppm) with H-1″ of the glutathionyl moiety (2.83 and 3.15 ppm) observed in the HMBC spectrum of daruricine-SG (Figure 5B) provides critical evidence to support the above interpretation of the COSY and HSQC spectra of dauricine-SG. The facts obtained from the NMR experiments along with LC-MS/MS studies allowed us to assign M6 as 17-glutathionyl dauricine. It is most likely that the GSH conjugate was formed by a reaction between GSH and the *p*-quinone methide of dauricine via 1,6-addition.

With retention times at 11.5 and 13.3 min, M7-1 and M7-2 had protonated molecule $[M + H]^+$ at *m/z* 916 and double charge ions $[M + 2H]^{2+}$ at *m/z* 459, respectively, which was

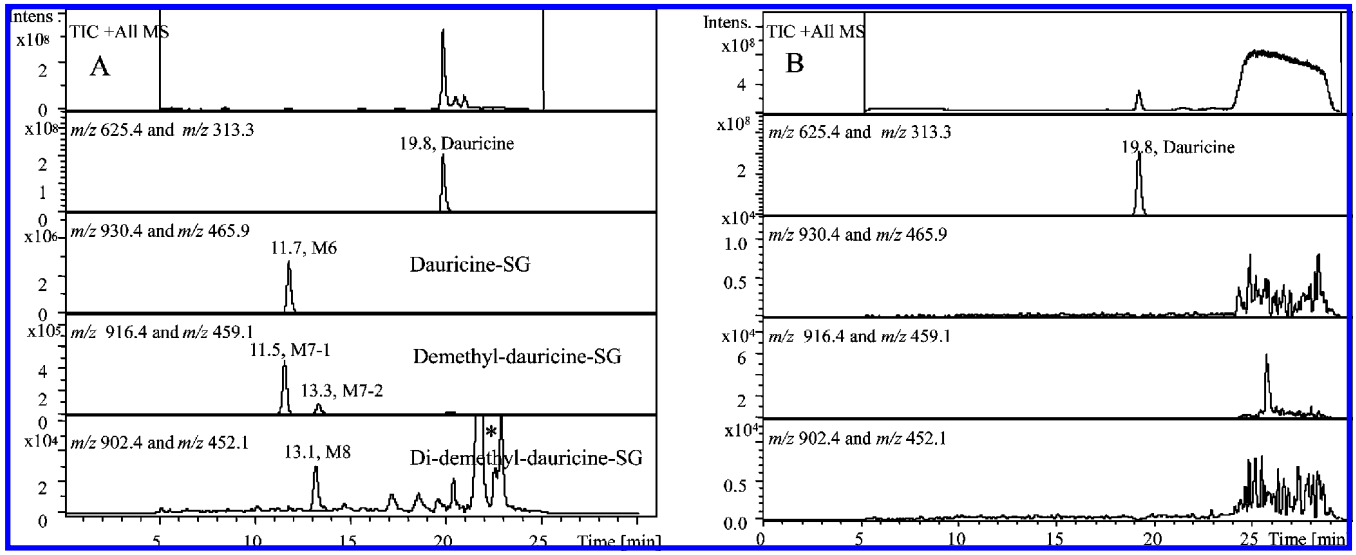

Figure 3. Extracted ion $[M + H]^+$ and $[M + 2H]^{2+}$ chromatograms of four conjugates in human liver microsomal incubations. (A) With NADPH and GSH; (B) with GSH but without NADPH. The detected metabolites are labeled as M6−M8, and the parent compound is labeled as dauricine. (*) The interference peaks at 21.5 and 23.0 min were derived from NADPH, corresponding to the abundant ion at *m/z* 452 (the ion at *m/z* 902 was not observed).

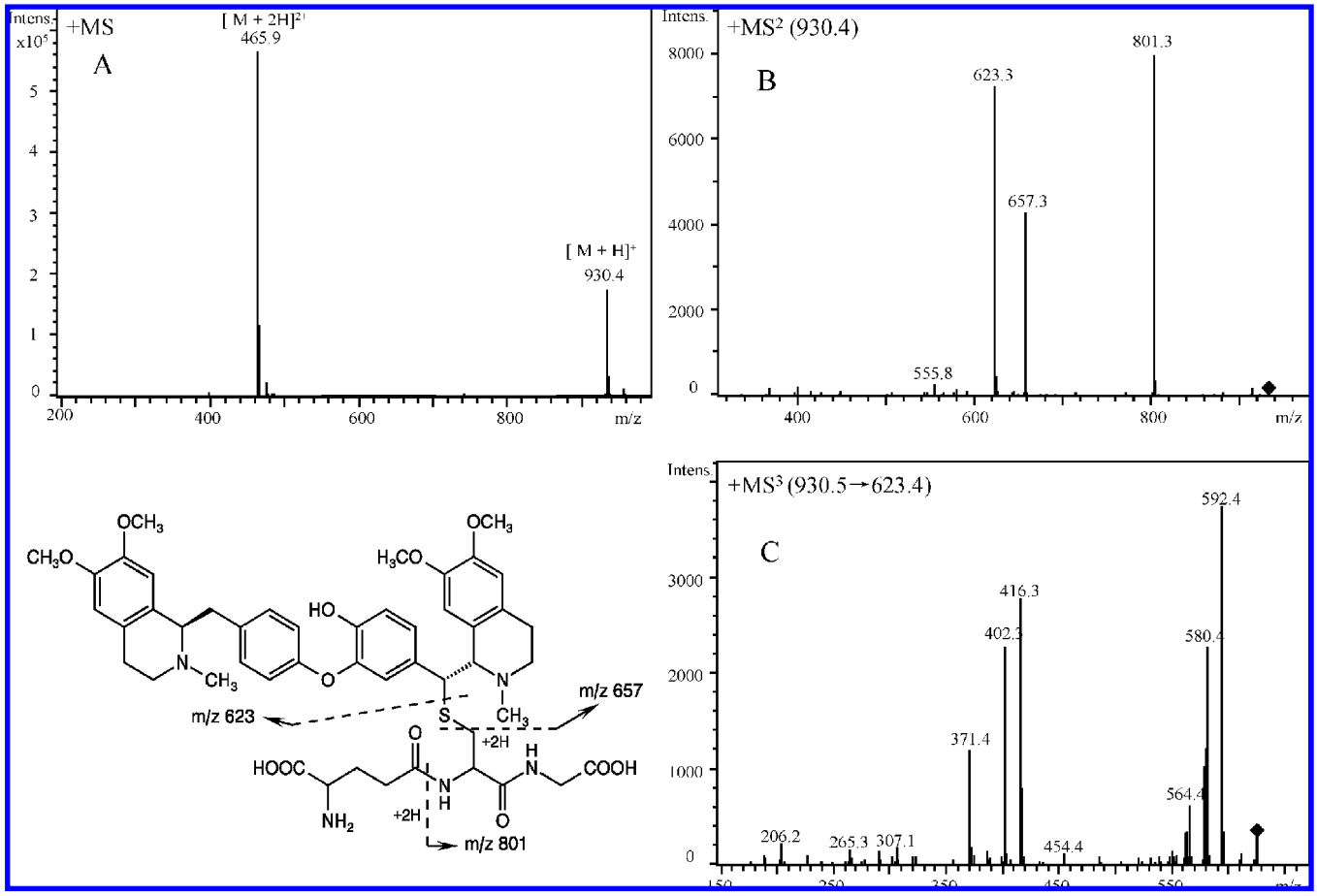

Figure 4. Mass spectrometry analysis of dauricine GSH conjugate (M6) in human liver microsomes. (A) Full scan mass spectrum; (B) MS/MS spectrum; and (C) MS^3 spectrum.

Table 2. Mass Spectral Data of Dauricine and Its GSH Conjugate (M6) Acquired by LTQ/Orbitrap Mass Spectrometry

				error		
	measured mass	calculated mass	formula	mDa	PPM	RDB
dauricine	625.3271	625.3272	$C_{38}H_{45}N_2O_6$	−0.1	−2.0	17.5
MS/MS (*m/z* 625)	594.2845	594.2850	$C_{37}H_{40}N_1O_6$	−0.5	−0.90	18.5
	582.2845	582.2850	$C_{36}H_{40}N_1O_6$	−0.5	−0.80	17.5
	260.1174	206.1176	$C_{12}H_{16}NO_2$	−0.2	−0.66	5.5
M6	930.3968	930.3954	$C_{48}H_{60}N_5O_{12}S$	−1.4	−1.5	21.5
MS/MS (*m/z* 930)	801.3517	801.3528	$C_{43}H_{53}N_4O_9S$	−1.1	−1.3	19.5
	657.2983	657.2993	$C_{38}H_{45}N_2O_6S$	−1.0	−1.5	17.5
	623.3103	623.3116	$C_{38}H_{43}N_2O_6$	−1.3	−2.0	18.5

Table 3. ^{1}H and ^{13}C-NMR Data of Dauricine and Its GSH Conjugate (M6) (δ in CD_3OD)

	proton signals		carbon signals	
	dauricine	M6	dauricine	M6
C-1	3.72 (1H, m)	4.57 (1H, d, J = 9.5 Hz)	66.2	68.3
C-17	Ha: 2.65 (1H, m)Hb: 3.15 (1H, m)	4.45 (1H, d, J = 9.5 Hz)	26.5	55.1
C-1′	3.72 (1H, m)	4.58 (1H, m)	65.9	66.3
C-17′	Ha: 2.65 (1H, m) Hb: 3.15 (1H, m)	Ha: 3.01 (1H, m) Hb: 3.54 (1H, m)	26.4	22.5
C-5	6.53 (1H, s)	6.71 (1H, s)	118	113
C-8	5.77 (1H, s)	5.89(1H, s)	113	114
C-5′	6.68 (1H, s)	6.92 (1H, s)	113	113
C-8′	5.86 (1H, s)	6.12 (1H, s)	113	114
C-10	6.68 (1H, d, J = 2.4 Hz)	6.62 (1H, bls)	127	124
C-13	6.91 (1H, d, J = 8.4 Hz)	7.06 (1H, d, J = 8.3 Hz)	130	119
C-14	6.89 (1H, dd, J = 8.4 and 2.4 Hz)	7.20 (1H, brd, J = 8.3 Hz)	132	128
C-11′,13′	6.68 (2H, d, J = 8.4 Hz)	6.76 (2H, d, J = 8.4 Hz)	118	118
C-10′,14′	6.95 (2H, d, J = 8.4 Hz)	7.13 (2H, d, J = 8.4 Hz)	124	132
C-1″		Ha: 2.83 (1H, d, J = 6.0 and 13 Hz) Hb: 3.15 (1H, d, J = 6.0 and 13 Hz)		34.2
C-2″		4.47 (1H, m)		54.1

305 Da higher than those of demethylated dauricine. This indicates that M7-1 and M7-2 were GSH conjugates derived from demethylated dauricine. The MS^n spectra of M7-1 and M7-2 showed identical fragment ions. The MS/MS spectrum

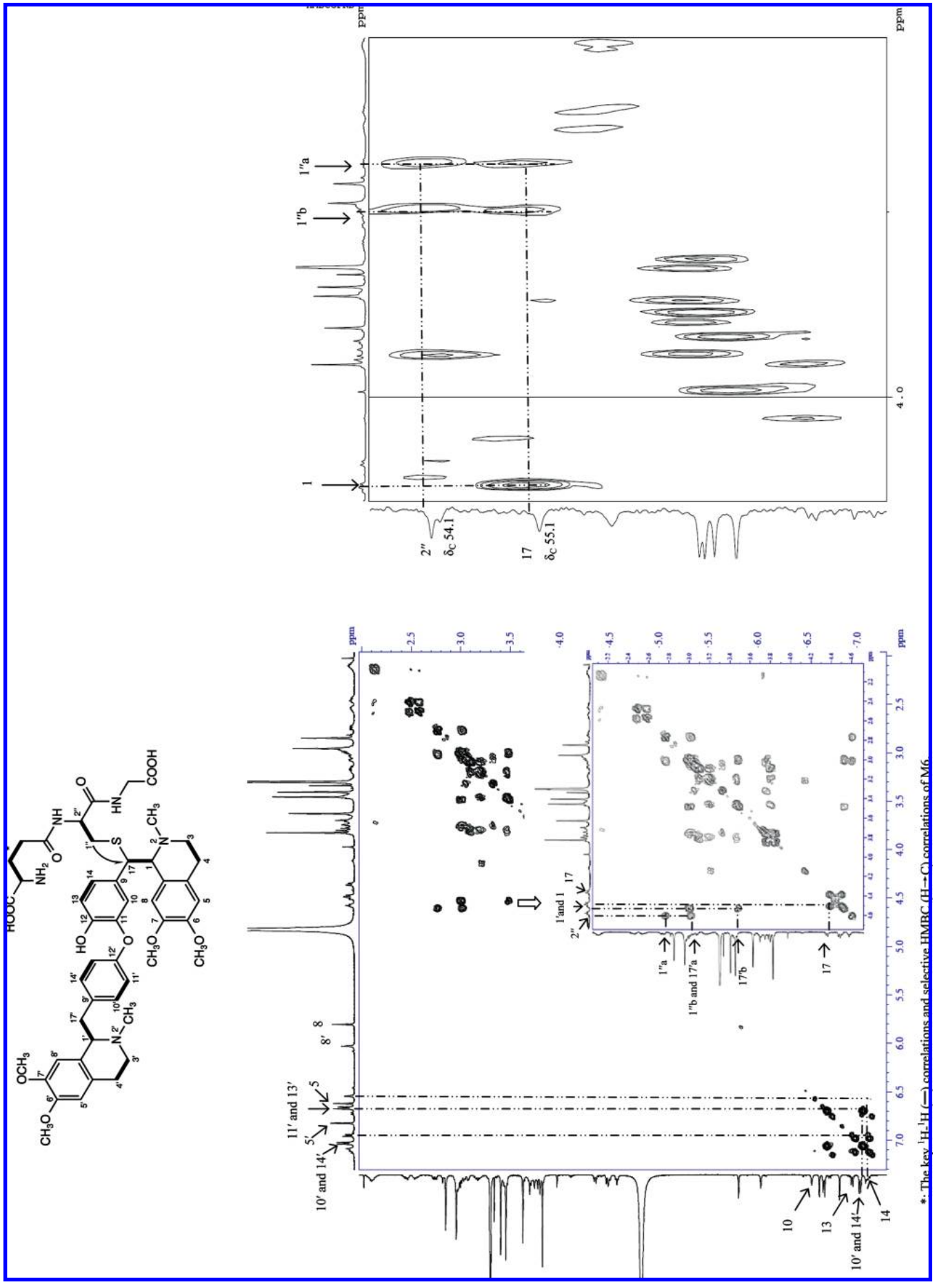

Figure 5. ^{1}H−^{1}H COSY (A) and section of HMBC (B) spectra of synthetic dauricine-SG. The inset is the expanded region for A.

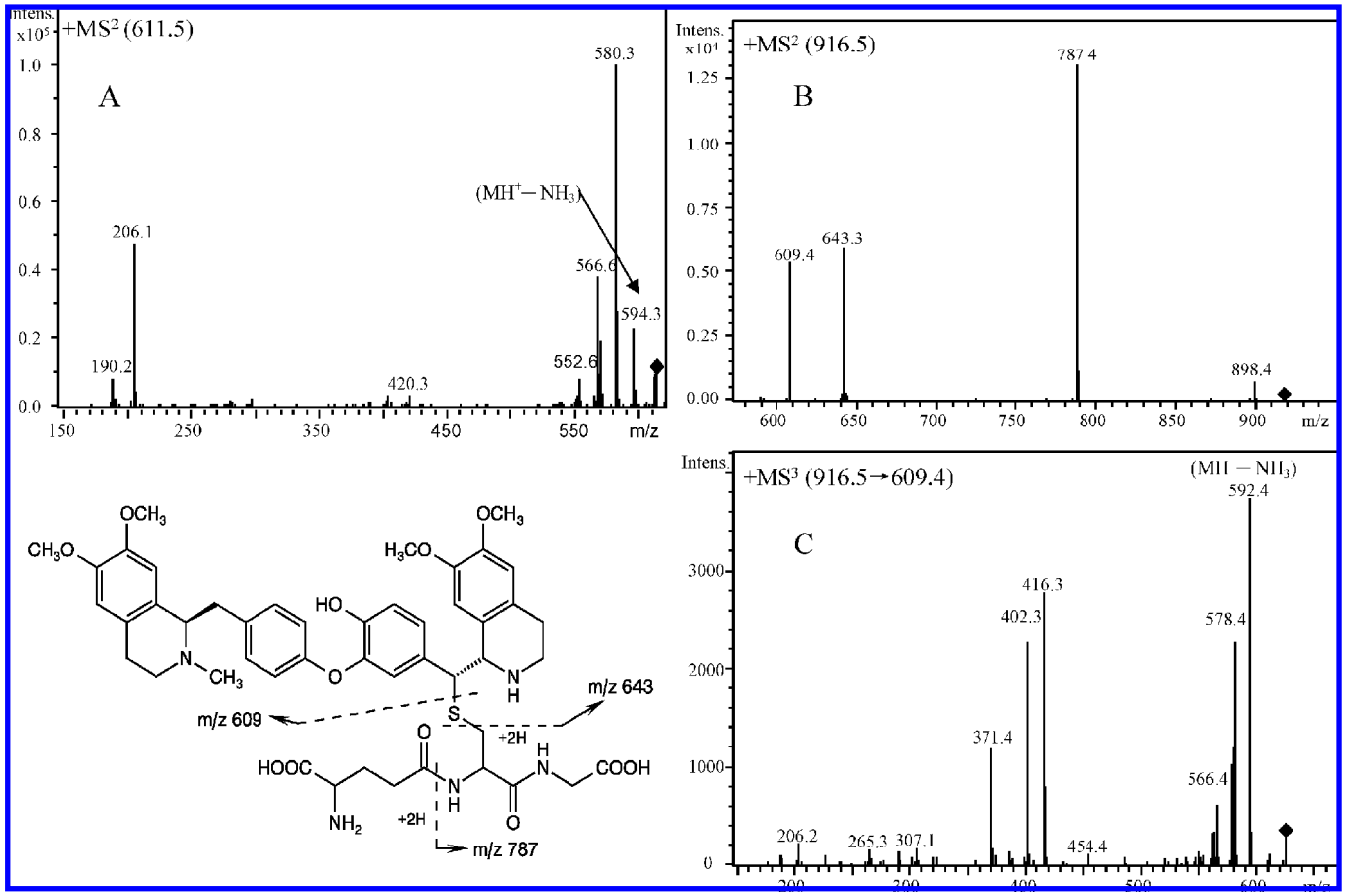

Figure 6. Mass spectrometry analysis of 2-*N*-demethyl dauricine (M3-3) and its GSH conjugate (M7-1) in human liver microsomes. (A) MS/MS spectrum of M3-3; (B) MS/MS spectrum of M7-1; and (C) MS^3 spectrum of M7-1.

displayed product ions of 787 (−129 Da, −pyroglutamate), 643 (−273 Da, −(GSH−H_2S)), and 609 (−307 Da, −GSH) (Figure. 6), and the MS^3 spectrum of the *m/z* 916→609 ion showed fragment ions at 592 (−17 Da, −NH_3), 578 (−31 Da, −CH_3NH_2), 564 (−43 Da, −$CH_3N{=}CH_2$), and 206 (Figure 6), where the neutral losses were coincident with those of MS/MS for *N*-demethyl dauricine (Figure 6). Authentic GSH conjugate derived from 2-*N*-demethyl dauricine was synthesized using the same method as that for the synthesis of M6. The synthetic product revealed the same retention time and fragment ions as those of M7-1 (data not shown). This allowed us to assign M7-1 as the GSH conjugate of 2-*N*-demethyl dauricine. Since there are only two tertiary amine atoms in the structure of dauricine, M7-2 was, by exclusion, characterized as the GSH conjugate derived from 2′-*N*-demethyl dauricine. We have not identified the exact structure of the synthetic GSH conjugate by NMR due to impurity. We are assuming that GSH was conjugated at C-17 just as for M6, and we are making a continuous effort to nail down the structure of M7-1.

Metabolite M8 at the retention time of 13.1 min showed a protonated molecule $[M + H]^+$ at *m/z* 902 and a double charge ion $[M + 2H]^{2+}$ at *m/z* 452, which was 305 Da higher than those of bis-demethyl dauricine. This indicates that M8 was a GSH conjugate derived from bis-demethyl dauricine. The MS/MS spectrum displayed product ions of 773 (−129 Da, −pyroglutamate), 629 (−273 Da, − (GSH −H_2S)), and 595 (−307 Da, −GSH) (Figure. 7), with the MS^3 spectrum showing the *m/z* 902→595 ion and fragment ions at 578 (−17 Da, −NH_3), and 564 (−31 Da, −CH_3NH_2) (Figure 7). Tentatively, M8 was assigned as a GSH conjugate of *N*-demethyl and *O*-demethyl dauricine due to the observed neutral loss of 17 Da (NH_3) and 31 Da (CH_3NH_2) in its MS^3 spectrum.

Enzymes Involved in the Formation of GSH Conjugates. We determined the enzymes responsible for the oxidative metabolism of dauricine by incubation of dauricine with individual recombinant human CYPs 1A2, 2A1, 2C9, 2C19, 2D6, 2E1, and 3A4, mixed with GSH as the trapping agent. Metabolites M6, M7-1, M7-2, and M8 were detected in GSH-fortified incubation only with CYP3A4. There were no such products detected in the incubation with the other isoforms. Additionally, the role of CYP3A4, 2A1, 2D6, 1A2, 2C9, and 2C19 in the bioactivation of dauricine was probed by isoenzyme-selective inhibitors, i.e., ketoconazole, pilocarpine, quinidine, α-naphthoflavone, sulfaphenazole, and ticlopidine coincubated with pooled human liver microsomes in the presence of GSH. Enzyme inhibition by individual inhibitors was confirmed using CYP450 marker substrates. As expected, ketoconazole, not the other inhibitors, significantly reduced the formation of the quinone methide metabolites (Figure 8). Also, the inhibitory effect was proportional to the concentrations of ketoconazole applied (Figure 8).

Consistent with the results obtained from the chemical inhibition studies in human liver microsomes, the K_m value in HLM (2.14 μM) incubations was similar to that in the incubations with recombinant CYP3A4 (2.58 μM), which further indicates the solo role of CYP3A4 in the formation of quinone methide metabolites from dauricine. The estimated V_{max} of 4.21 pmol/min/mg protein and 40.3 pmol/min/nmol 3A4 were found for HLM and CYP3A4, respectively.

Excretion of Dauricine-Derived GSH Conjugates in Rat Bile. Oxidative bioactivation of dauricine was further

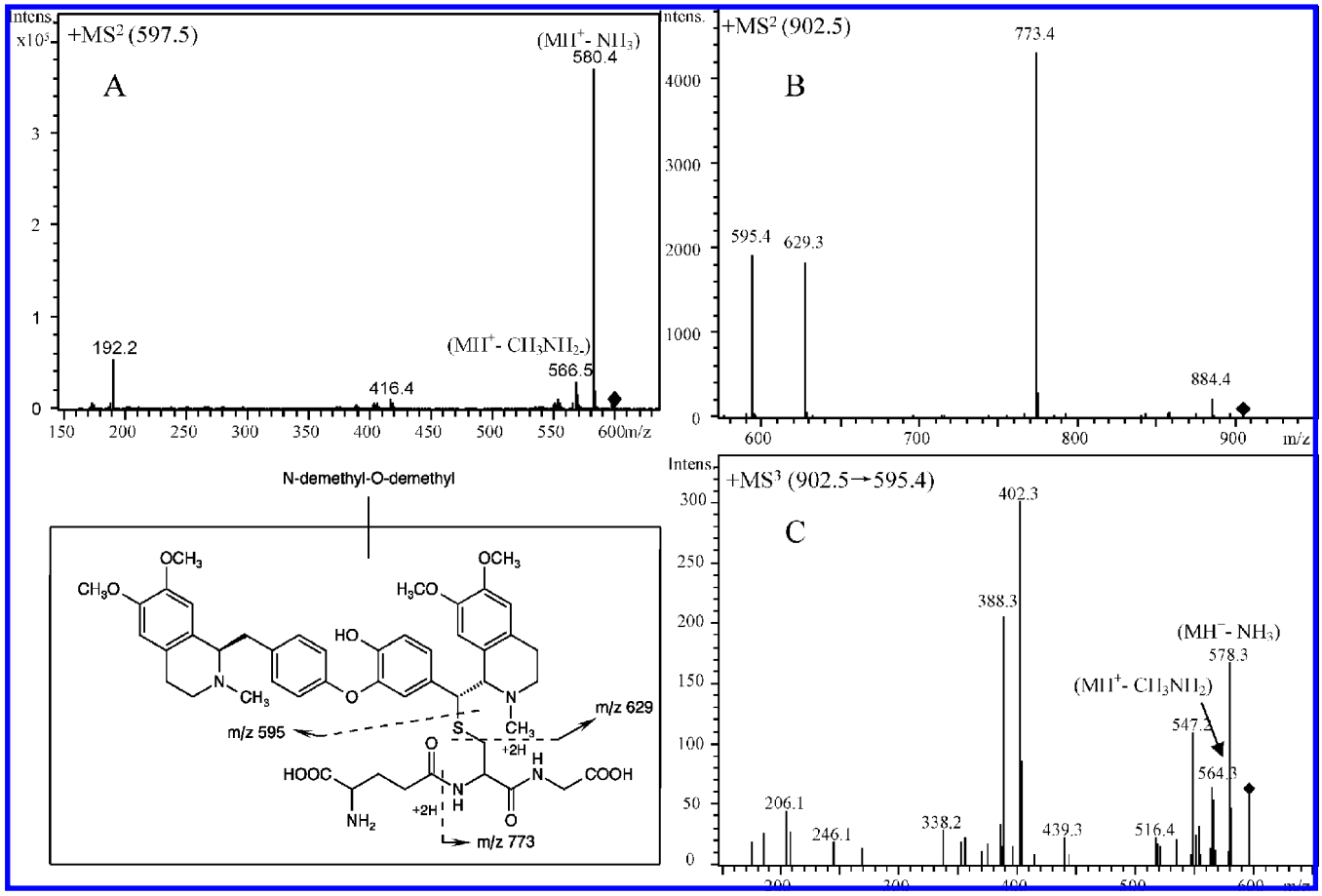

Figure 7. Mass spectrometry analysis of *O*-demethyl-*N*-demethyl dauricine (M4) and its GSH conjugate (M8) in human liver microsomes. (A) MS/MS spectrum of M4; (B) MS/MS spectrum of M8; and (C) MS^3 spectrum of M8.

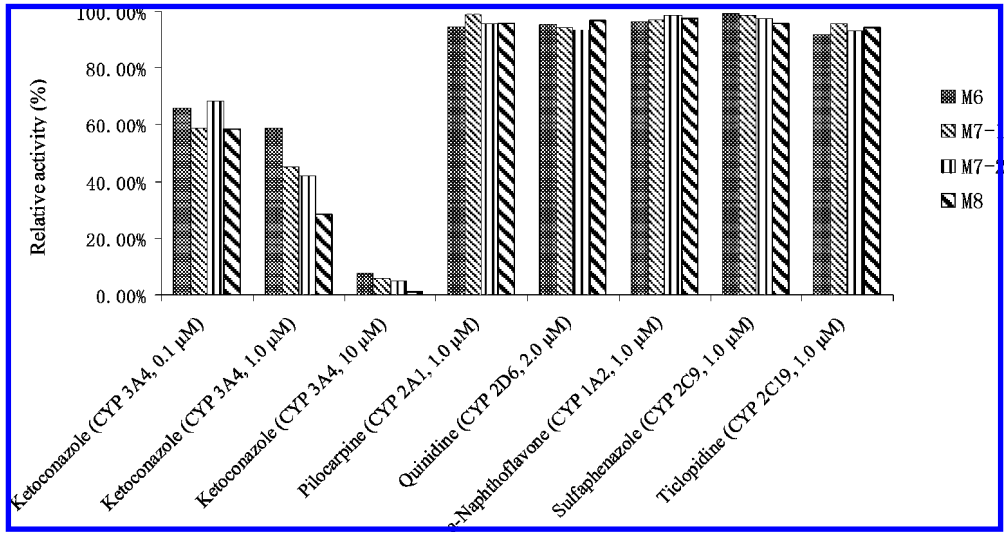

Figure 8. Effect of isozyme-selective CYP450 inhibitors on the formation of GSH conjugates M6, M7-1, M7-2, and M8 in incubations of dauricine with human liver microsomes. Data are reported as the mean of two separate determinations.

studied in vivo by examining the biliary excretion of GSH conjugates derived from dauricine after an oral dose of 40 mg/kg in rats. Three GSH conjugates, identical with those observed in human liver microsomal incubation studies, were detected in rat bile by LC/MS^n analysis. They were GSH conjugates derived from dauricine (M6), 2-*N*-demethyl dauricine (M7-1) and 2′-*N*-demethyl dauricine (M7-2) as shown in the Supporting Information (Figure S3). The GSH conjugate of *N*-demethyl-*O*-demethyl dauricine (M8) was not found in rat bile (Figure S3, Supporting Information).

Discussion

Dauricine contains a *para*-methylene phenol moiety in its structure, which might be metabolized to quinone methide intermediates. These reactive metabolites could be trapped by

Scheme 2. Proposed Mechanism for the Formation of Four GSH Conjugates from Dauricine and Its Metabolites in Human Liver Microsomal Incubations Supplemented with NADPH and GSH

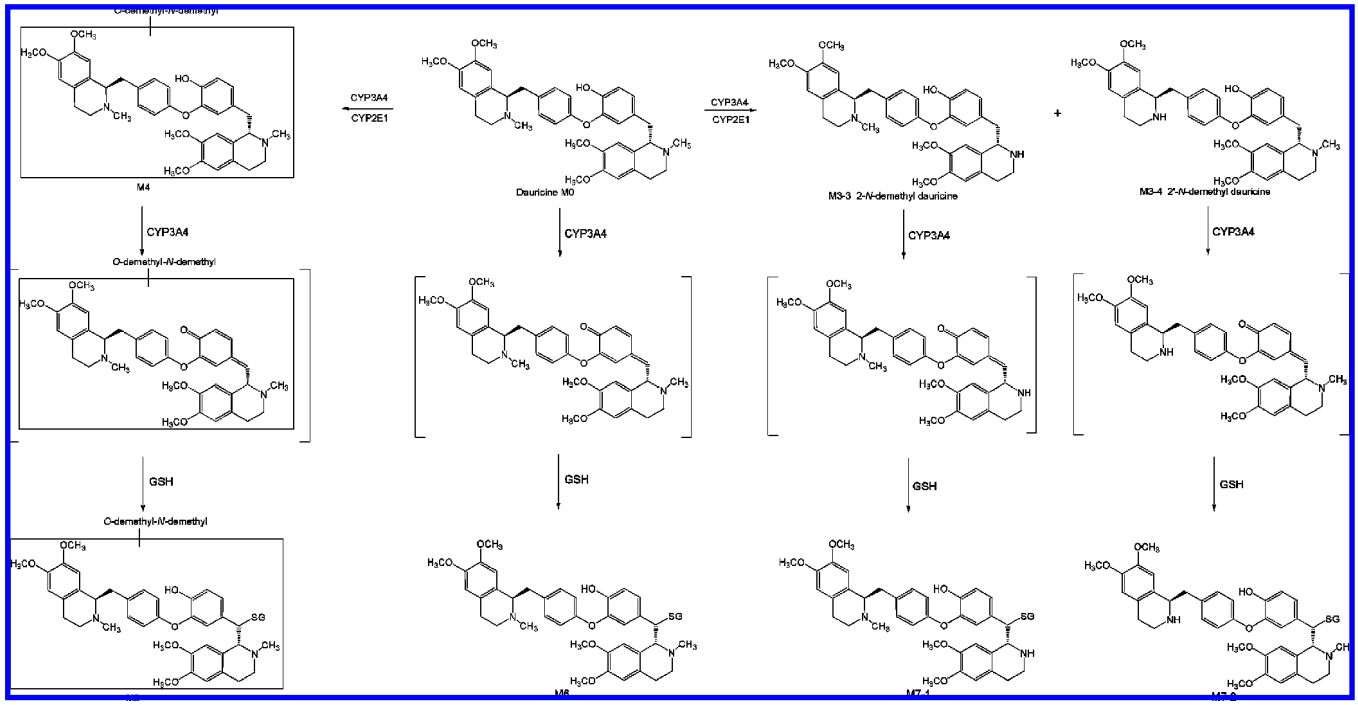

nucleophilic agents such as glutathione. A screen for the formation of GSH conjugates could potentially identify a significant portion of electrophilic metabolites formed from a chemical in vivo and in vitro. In the present study, four novel GSH conjugates of dauricine were identified following human liver microsomal incubations of dauricine in the presence of NADPH and GSH, three of which were also detected in rat bile after an oral dose of 40 mg/kg dauricine. The formation of the GSH conjugates was found to require NADPH, and the absence of NADPH in human liver microsomal incubations failed to produce any GSH conjugates after exposure to dauricine.

In LC/MS^n analysis, the characteristic fragmentation mainly results from the cleavage of peptide backbone of the glutathione moiety (*18, 19*). For metabolites M6 to M8, their MS/MS spectra shared the same feature of the neutral losses of 129 Da (pyroglutamate), 273 Da (GSH − H_2S), and 307 Da (GSH). In order to characterize parent moieties of GSH conjugates, the MS^3 spectra of the ions at $[MH - 307\ Da]^+$ allowed us to narrow down the site of biotransformation by monitoring the fragmentation patterns, which reflects the advantage of ion trap mass spectrometry (*20, 21*). In the MS^3 spectra of M6 to M8 ($MH \rightarrow [MH - 307\ Da]^+$), 31 Da ($CH_3NH_2$) and 43 Da ($CH_3N{=}CH_2$) were the common neutral losses, and the neutral loss of NH_3 (17 Da) appeared at M7-1, M7-2, and M8, indicating that they contained one *N*-demethylated moiety in their structures. On the basis of MS data, the identities of the four GSH conjugates were finalized as GSH conjugates derived from dauricine (M6), 2-*N*-demethyl dauricine (M7-1), 2′-*N*-demethyl dauricine (M7-2), and *N*-demthyl-*O*-demethyl dauricine (M8).

To confirm the absolute structures of these detected GSH conjugates, attempts were made to synthesize the authentic standard by oxidizing dauricine with DDQ, followed by conjugating with GSH. By MS^n in combination with NMR analysis of the synthetic conjugate, M6 was characterized as 17-glutathionyl dauricine. The ^1H NMR, ^{13}C NMR, ^1H-^1H COSY, HSQC, and HMBC spectral studies on the synthetic GSH conjugate of dauricine suggested that the structural integrity of the *p*-hydroxyphenyl ring likely was preserved and that the site of GSH addition was the benzylic carbon (C-17). We assume that the other three GSH conjugates, including M7-1, M7-2, and M8, share the same regionchemistry and hold the glutathionyl group at C-17.

All incubations in this study were performed under aerobic conditions. The formation of NADPH-dependent GSH conjugates indicated that one or more CYP450s were involved in the production of the reactive intermediates by human liver microsomes. Experiments with recombinant CYP enzymes revealed that only CYP3A4 mediated the formation of GSH conjugates M6 to M8 when GSH was present in the incubation mixtures. The incubation of dauricine with individual chemical inhibitors, GSH, and pooled human liver microsomes also indicated that CYP3A4 played a major role in the formation of quinone methide metabolites of dauricine. Similar K_m values for the formation of the quinone methide metabolite of dauricine were observed when incubated with either human liver microsomes or recombinant CYP3A4 enzyme. The demethylation of dauricine was primarily catalyzed by CYP3A4, with a minor contribution from CYP2E1. The metabolic pathways are proposed in Scheme 2.

It has been reported that *ortho*- or *para*-alkyl-substituted phenols can undergo π-oxidation to quinone methide intermediates, capable of reacting with nucleophiles, including proteins and/or DNA in vivo, which could cause a variety of toxic effects such as acute cytotoxicity and carcinogenesis (*22*−*28*). The finding of quinone methide metabolites in microsomal incubations of dauricine sounded an alarming note for the safe consumption of dauricine-related natural products, and the toxic effects of dauricine are under investigation.

In summary, dauricine is subject to oxidative bioactivation in vitro with human liver microsomes and in vivo in rats. The formation of quinone methide metabolites is inferred from the structures of their GSH conjugates detected in rat bile and human liver microsomal incubations supplemented with GSH. Isoform CYP3A4 played a primary role in the generation of the quinone methide metabolites. The finding of the chemically reactive

metabolites would draw great attention to the safety of dauricine consumption.

Acknowledgment. This work was supported by Grant # 30873119 of the National Natural Science Foundation of China. We thank Dr. Jianbo Qu at Shandong University (Jinan, China) for helpful discussions of the NMR data.

Supporting Information Available: ^{1}H NMR, ^{13}C NMR, and ^{1}H-^{1}H COSY spectra of dauricine, HSQC spectrum of synthetic dauricine-SG, and extracted ion $[M + H]^+$ and $[M + 2H]^+$ chromatograms of dauricine and its GSH conjugates in bile sample after an oral dose of 40 mg/kg to a rat. This material is available free of charge via the Internet at http://pubs.acs.org.

References

(1) Angerhofer, C. K., Guinaudeau, H., Wongpanich, V., Pezzuto, J. M., and Cordell, G. A. (1999) Antiplasmodial and cytotoxic activity of natural bisbenzylisoquinoline alkaloids. *J. Nat. Prod. 62*, 59–66.

(2) Marshall, S. J., Russell, P. F., Wright, C. W., Anderson, M. M., Phillipson, J. D., Kirby, G. C., Warhurst, D. C., and Schiff, P. L., Jr. (1994) In vitro antiplasmodial, antiamoebic, and cytotoxic activities of a series of bisbenzylisoquinoline alkaloids. *Antimicrob. Agents Chemother. 38*, 96–103.

(3) He, Q. Y., Meng, F. H., and Zhang, H. Q. (1996) Reduction of doxorubicin resistance by tetrandrine and dauricine in harringtonine-resistant human leukemia (HL60) cells. *Acta Pharmacol. Sin. 17*, 179–181.

(4) Lohombo-Ekomba, M. L., Okusa, P. N., Penge, O., Kabongo, C., Choudhary, M. I., and Kasende, O. E. (2004) Antibacterial, antifungal, antiplasmodial, and cytotoxic activities of *Albertisia villosa*. *J. Ethnopharmacol. 93*, 331–335.

(5) Zhao, X., Cui, X. Y., Chen, B. Q., Chu, Q. P., Yao, H. Y., Ku, B. S., and Zhang, Y. H. (2004) Tetrandrine, a bisbenzylisoquinoline alkaloid from Chinese herb Radix, augmented the hypnotic effect of pentobarbital through serotonergic system. *Eur. J. Pharmacol. 506*, 101–105.

(6) Li, Y. H., and Gong, P. L. (2007) Neuroprotective effect of dauricine in cortical neuron culture exposed to hypoxia and hypoglycemia: involvement of correcting perturbed calcium homeostasis. *Can. J. Physiol. Pharmacol. 85*, 621–627.

(7) Li, Y. H., and Gong, P. L. (2007) Neuroprotective effects of dauricine against apoptosis induced by transient focal cerebral ischaemia in rats via a mitochondrial pathway. *Clin. Exp. Pharmacol. Physiol. 34*, 177–184.

(8) Lin, H., Wang, Y., Xiong, Z., Tang, Y., and Liu, W. (2007) Effect of antenatal tetrandrine administration on endothelin-1 and epidermal growth factor levels in the lungs of rats with experimental diaphragmatic hernia. *J. Pediatr. Surg. 42*, 1644–1651.

(9) Yang, X. Y., Jiang, S. Q., Zhang, L., Liu, Q. N., and Gong, P. L. (2007) Inhibitory effect of dauricine on inflammatory process following focal cerebral ischemia/reperfusion in rats. *Am. J. Chin. Med. 35*, 477–486.

(10) Du, Z. H., Liu, H. G., Chai, C. Y., Luo, L. Y., and Hu, C. J. (1986) Anti-inflammatory effect of dauricine. *Zhongguo Yao Li Xue Bao 7*, 419–422.

(11) Qian, J. Q. (2002) Cardiovascular pharmacological effects of bisbenzylisoquinoline alkaloid derivatives. *Acta Pharmacol. Sin. 23*, 1086–1092.

(12) Xia, J. S., Guo, D. L., Zhang, Y., Zhou, Z. N., Zeng, F. D., and Hu, C. J. (2000) Inhibitory effects of dauricine on potassium currents in guinea pig ventricular myocytes. *Acta Pharmacol. Sin. 21*, 60–64.

(13) Xia, J. S., Li, Z., Dong, J. W., Tu, H., and Zeng, F. D. (2002) Dauricine-induced changes in monophasic action potentials and effective refractory period of rabbit left ventricle in situ. *Acta Pharmacol. Sin. 23*, 371–375.

(14) Chen, S., Liu, L., Yang, Y., Dai, Z., and Zeng, F. (2000) Metabolism of dauricine and identification of its main metabolites. *J. Tongji. Med. Univ. 20*, 253–256.

(15) Han, F. M., Peng, Z. H., Song, W., Zhang, H. M., Zhu, M. M., and Chen, Y. (2007) Identification of dauricine and its metabolites in rat urine by liquid chromatography-tandem mass spectrometry. *J.Chromatogr., B 854*, 1–7.

(16) Becker, H. D., and Gustafsson, K. (1976) Preparation and reactions of 2,6-di-tert-butyl-4-(9-fluorenylidene)-1,4-benzoquinone. *J. Org. Chem. 41*, 214–221.

(17) U.S. Department of Health and Human Service, Food and Drug Administration. (2006) Guidance for Industry on Drug Interaction Studies. http://www.fda.gov/cder/guidelines.htm (accessed September 2006).

(18) Ma, S. G. and Chowdhury, S. K. (2007) Application of liquid chromatography/mass spectrometry for metabolite identification. In *Drug Metabolism in Drug Design and Development* (Zhang, D. L., Zhu, M. S., and Humphreys, W. G., Eds.) pp 354–357.

(19) Yao, M., Ma, L., Humphreys, W. G., and Zhu, M. (2008) Rapid screening and characterization of drug metabolites using a multiple ion monitoring-dependent MS/MS acquisition method on a hybrid triple quadrupole-linear ion trap mass spectrometer. *J. Mass. Spectrom. 80*, 1788–1799.

(20) Gan, J., Hsueh, M. M., Qu, Q., Harper, T. W., and Humphreys, W. G. (2005) Dansyl glutathione as a trapping agent for the quantitative estimation and identification of reactive metabolites. *Chem. Res. Toxicol. 18*, 896–903.

(21) Korfmacher, W. (2005) *Using Mass Spectrometry for Drug Metabolism Studies*, Chapter 8, CRC Press, Boca Raton, FL.

(22) Bolton, J. L., Trush, M. A., Penning, T. M., Dryhurst, G., and Monks, T. J. (2000) Role of quinones in toxicology. *Chem. Res. Toxicol. 13*, 135–160.

(23) Monks, T. J., and Jones, D. C. (2002) The metabolism and toxicity of quinones, quinonimines, quinone methides and quinone-thioethers. *Curr. Drug. Metab. 3*, 425–438.

(24) Baillie, T. A. (2008) Metabolism and toxicity of drugs. Two decades of progress in industrial drug metabolism. *Chem. Res. Toxicol. 21*, 129–137.

(25) Reilly, C. A., and Yost, G. S. (2006) Metabolism of capsaicinoids by P450 enzymes: a review of recent findings on reaction mechanisms, bio-activation, and detoxification processes. *Drug Metab. Rev. 38*, 685–706.

(26) Bender, R. P., Lindsey, R. H. J., Burden, D. A., and Osheroff, N. (2004) N-Aceyl-*p*-benzoquinone imine, the toxic metabolite of acetaminophen, is a topoisomerase II poison. *Biochemistry 43*, 3731–3739.

(27) Lindsey, R. H. J., Bender, R. P., and Osheroff, N. (2005) Effect of benzene metabolites on DNA cleavage mediated by human topoisomerase IIα: 1, 4-hydroquinone is a topoisomerase II poison. *Chem. Res. Toxicol. 18*, 761–770.

(28) Thompson, D. C., Perera, K., Krol, E. S., and Bolton, J. L. (1995) o-Methoxy-4-alkylphenols that form quinone methides of intermediate reactivity are the most toxic in rat liver slices. *Chem. Res. Toxicol. 8*, 323–327.

TX800397E